

Echo time dependence of biexponential and triexponential intravoxel incoherent motion parameters in the liver

Tobit Führes¹  | Andreas Julian Riexinger¹  | Martin Loh¹ | Jan Martin² |
Andreas Wetscherek³ | Tristan Anselm Kuder⁴ | Michael Uder¹ | Bernhard Hensel⁵ |
Frederik Bernd Laun¹

¹Institute of Radiology, University Hospital Erlangen, Friedrich-Alexander-Universität Erlangen-Nürnberg (FAU), Erlangen, Germany

²Lund University, Lund, Sweden

³Joint Department of Physics, The Institute of Cancer Research and The Royal Marsden NHS Foundation Trust, London, United Kingdom

⁴Department of Medical Physics in Radiology, German Cancer Research Center (DKFZ), Heidelberg, Germany

⁵Center for Medical Physics and Engineering, Friedrich-Alexander-Universität Erlangen-Nürnberg (FAU), Erlangen, Germany

Correspondence

Tobit Führes, Institute of Radiology,
University Hospital Erlangen, Friedrich-
Alexander-Universität Erlangen-Nürnberg
(FAU), Maximiliansplatz 3, D-91054
Erlangen, Germany.
Email: tobit.fuehres@uk-erlangen.de

Funding information

Deutsche Forschungsgemeinschaft, Grant/
Award Number: LA 2804/12-1 and LA
2804/13-1; Vetenskapsrådet, Grant/
Award Number: 2018-03697; Stiftelsen
för Strategisk Forskning, Grant/Award
Number: ITM17-0267

Purpose: Intravoxel incoherent motion (IVIM) studies are performed with different acquisition protocols. Comparing them requires knowledge of echo time (TE) dependencies. The TE-dependence of the biexponential perfusion fraction f is well-documented, unlike that of its triexponential counterparts f_1 and f_2 and the biexponential and triexponential pseudodiffusion coefficients D^* , D_1^* , and D_2^* . The purpose was to investigate the TE-dependence of these parameters and to check whether the triexponential pseudodiffusion compartments are associated with arterial and venous blood.

Methods: Fifteen healthy volunteers (19–58 y; mean: 24.7 y) underwent diffusion-weighted imaging of the abdomen with 24 b-values (0.2–800 s/mm²) at TEs of 45, 60, 75, and 90 ms. Regions of interest (ROIs) were manually drawn in the liver. One set of bi- and triexponential IVIM parameters per volunteer and TE was determined. The TE-dependence was assessed with the Kruskal-Wallis test.

Results: TE-dependence was observed for f ($P < .001$), f_1 ($P = .001$), and f_2 ($P < .001$). Their median values at the four measured TEs were: f : 0.198/0.240/0.274/0.359, f_1 : 0.113/0.139/0.146/0.205, f_2 : 0.115/0.155/0.182/0.194. D , D^* , D_1^* , and D_2^* showed no significant TE-dependence. Their values were: diffusion coefficient D (10⁻⁴ mm²/s): 9.45/9.63/9.75/9.41, biexponential D^* (10⁻² mm²/s): 5.26/5.52/6.13/5.82, triexponential D_1^* (10⁻² mm²/s): 1.73/2.91/2.25/2.51, triexponential D_2^* (mm²/s): 0.478/1.385/0.616/0.846.

Conclusion: f_1 and f_2 show similar TE-dependence as f , ie, increase with rising TE; an effect that must be accounted for when comparing different studies. The diffusion and pseudodiffusion coefficients might be compared without TE correction. Because

This is an open access article under the terms of the Creative Commons Attribution License, which permits use, distribution and reproduction in any medium, provided the original work is properly cited.

© 2021 The Authors. *Magnetic Resonance in Medicine* published by Wiley Periodicals LLC on behalf of International Society for Magnetic Resonance in Medicine

of the similar TE-dependence of f_1 and f_2 , the triexponential pseudodiffusion compartments are most probably not associated to venous and arterial blood.

KEYWORDS

diffusion, echo time, IVIM, liver, perfusion

1 | INTRODUCTION

The intravoxel incoherent motion (IVIM) model described by Le Bihan et al. in 1986 treats the measured diffusion-weighted signal as a two-compartment model consisting of a diffusion and a perfusion compartment.¹ IVIM imaging has proved useful for detecting and staging various pathologies in many parts of the human body, such as the brain and abdominal organs.²

In the biexponential IVIM model, the signal decay as a function of the diffusion weighting b is described by a biexponential function, representing the summed signal of perfusion and diffusion compartments:

$$S = S_0 \cdot ((1 - f) \exp(-bD) + f \exp(-bD^*)). \quad (1)$$

S_0 denotes the unweighted signal strength, f the perfusion signal fraction, D the tissue diffusion coefficient, and D^* the pseudodiffusion coefficient.

However, it has been shown that the biexponential signal representation is not well-suited for describing the signal decay at small b -values in some organs, such as the liver³⁻⁶ and the kidney.⁷⁻¹¹ The observation of a very steep signal decay at very small diffusion weightings made it necessary to reformulate the biexponential signal representation into a triexponential one, the additional “compartment” describing a “faster” perfusion:

$$S = S_0 \cdot ((1 - f_1 - f_2) \exp(-bD) + f_1 \exp(-bD_1^*) + f_2 \exp(-bD_2^*)). \quad (2)$$

Here, the term describing the perfusion has been replaced by the sum of two perfusion terms, described by their respective signal fractions f_1 and f_2 and their pseudodiffusion coefficients D_1^* and D_2^* . No consensus has been reached regarding the tissue types and physiological functions to which these two compartments correspond.^{5,7} We follow the notion outlined by Riexinger et al.,⁵ and consider the two perfusion terms in Equation (2) as a data representation¹² rather than representing a biophysical model.

The determination of the IVIM parameters f and, in particular, D^* was found to be challenging.¹³⁻¹⁵ The high uncertainty in the pseudodiffusion coefficient results in a reduced

discriminatory value,^{16,17} eg, in the differentiation of subtypes of renal neoplasms,¹⁸ or between hepatocellular carcinoma (HCC) and focal nodular hyperplasia (FNH).¹⁹ Despite these difficulties, significant differences in the pseudodiffusion coefficient between pathologies were reported.^{20,21} For example, benign, intermediate, and malignant solid soft-tissue tumors were reported to have significantly different pseudodiffusion coefficients.²² Further, D^* is significantly decreased in fibrous meningioma compared to other meningioma.²³ Recently, the triexponential IVIM approach has also been used for disease characterization.^{8,9}

IVIM studies of the liver have been performed with a variety of echo times (TEs). For example, the following values have been used: 55 ms,⁴ 72 ms,²⁴ 100 ms,⁵ 120 ms.²⁵ Regarding this range of values, the question arises whether there is a dependency of the IVIM parameters on the choice of TE. If this was the case, the discriminatory value of IVIM parameters would have to be, if not even questioned, at least reassessed in consideration of the used TE. It is already well-known that the biexponential perfusion fraction f shows a strong dependency on TE in the liver²⁶ and pancreas,²⁷ which are organs of relatively short T_2 time. However, besides a conference report,²⁸ we are not aware of a study that evaluated whether such a TE dependency exists for the other bi- and triexponential IVIM parameters by acquiring data with different TEs but otherwise fixed settings.

In light of the above described increasing body of evidence that examinations of pseudodiffusion can reveal important information,^{22,29} and anticipating that this also holds true for triexponential IVIM parameters, our study was aimed at investigating the dependency of all biexponential and triexponential IVIM parameters on TE, intentionally without using a T_2 correction in the IVIM equation,^{26,27} in order to detect the influence on the mere IVIM parameters as they are used in other studies.

A secondary aim is to examine whether the two triexponential perfusion compartments could represent arterial and venous blood by considering their different T_2 times,^{30,31} which would alter their signal contribution depending on TE. Given the above-mentioned difficulties in fitting all IVIM parameters, we focused on the liver because it can be investigated well given its size and its large perfusion fraction.^{15,27}

2 | METHODS

2.1 | Data acquisition

All data were acquired with a 3T scanner (MAGNETOM Prisma, Siemens Healthineers, Erlangen, Germany) using an in-house developed single refocused spin-echo echo-planar imaging diffusion sequence.^{25,32} An 18-channel body coil and the built-in spine coil were used. Guided by an optimization for triexponential IVIM in the liver,¹⁴ diffusion-weighted images were recorded at the following 24 b-values: 0.2 s/mm² (two repetitions), 0.3 s/mm², 0.4 s/mm², 0.6 s/mm², 1 s/mm², 1.5 s/mm², 2 s/mm², 3.5 s/mm², 5 s/mm², 6 s/mm² (two repetitions), 10 s/mm², 25 s/mm², 35 s/mm², 45 s/mm², 60 s/mm², 70 s/mm², 80 s/mm², 200 s/mm² (two repetitions), and 800 s/mm² (three repetitions). A relatively large number of small b-values was used in order to correctly sample the initial steep signal decay (c.f. Supporting Information Figure S1 of Ref. [14]). These b-values were calculated numerically based on the gradient timetable, taking into account imaging gradient pulses.³³ For each b-value, six different diffusion encoding directions were used; (1,1,0), (-1,1,0), (0,1,1), (0, -1,1), (1,0,1), and (1,0, -1), specified in the scanner coordinate system. The numerically calculated b-values differed slightly between the six diffusion directions; therefore, the exact b-value of each diffusion direction was used in the evaluation. This means that six data points with slightly different b-values were used instead of a single data point at the respective nominal b-value. These data were acquired for TE = 45 ms, 60 ms, 75 ms, and 90 ms. The time Δ between the onsets of the two gradient pulses and the diffusion gradient pulse duration δ were kept constant at 21.64 ms and 12.24 ms, respectively, for all TEs.

For the phantom measurement, a vendor-provided bottle phantom filled with saline solution (per 1000 g H₂O: 3.75 g NiSO₄ × 6 H₂O, 5 g NaCl) was used. The same protocol was used for the phantom and the volunteer measurements. The temperature was measured with a BOSCH PTD 1 infrared thermometer (Robert Bosch Power Tools GmbH, Stuttgart, Germany). The aim of the phantom measurement was to perform a quality check of the in-house developed sequence.

Fifteen healthy volunteers (age range: 19-58 y, mean age: 24.7 y, median age: 23 y, male/female: 7/8, no known history of liver diseases) were scanned in supine position. Six transversal slices with 4-mm thickness and 4-mm spacing between slices were placed in the liver. Triggering was done in expiration using an external respiratory trigger. Other sequence parameters were field of view (FOV) 400 mm × 400 mm, matrix size 100 × 100 (interpolated to 200 × 200), GRAPPA (acceleration factor 2, 24 reference lines), phase direction anterior-posterior, phase partial Fourier factor 6/8, fat saturation mode: gradient reversal and spectral attenuated inversion recovery (SPAIR), acquisition bandwidth 2272 Hz/

Px, echo spacing 0.5 ms, repetition time (TR) = 1 respiratory cycle. The vendor-provided pre-scan normalize option was used to compensate for surface coil flare. The total acquisition time depended on the volunteers' respiratory frequency and was about 60 min for all TEs and b-values. The study was approved by the Institutional Ethics Committee, and written informed consent was obtained from all volunteers.

2.2 | Determination of the IVIM parameters

Data analysis was performed using in-house software developed with MATLAB R2017b (The MathWorks Inc., Natick, MA, USA). The signals of each TE were evaluated separately. For each slice of each TE, a single region of interest (ROI) excluding large vessels was defined on a b = 35 s/mm² image and afterward verified, and if necessary, corrected on a b = 0.2 s/mm² image. This procedure was chosen because we found it easier to identify and exclude large vessels when blood appeared dark. The left liver lobe was omitted to avoid bias due to the cardiac pulsation artifact, which is more pronounced in the left liver lobe than in the right liver lobe.³⁴⁻³⁶ Then, the ROI was copied to the images acquired with the other diffusion directions and b-values. The median signal in the ROI was calculated for each acquired image. The median instead of the mean was used to render the evaluation more stable and robust against outliers. These thus calculated signals were normalized to the signal of the lowest b-value. Because the lowest b-value was measured twice and with 6 diffusion encoding directions each, its signal was calculated as the mean signal of all 12 measurements. The normalized data of all slices of each volunteer were used together to fit the IVIM parameters to them, treating the signals of all acquired images (ie, all used diffusion directions for all diffusion weightings) as equally weighted data points. Because S_0 was also fitted (see below), the main purpose of the normalization was to allow a straightforward comparison of fitted curves.

For the phantom measurement, the diffusion coefficient was determined with a monoexponential fit function. The provided error of the diffusion coefficient was the standard error, which was given by the fit algorithm.

For the volunteer measurement, the fit was performed in two steps. A nonlinear least squares fit using the trust-region algorithm was used for each step. The objective function was the sum of squared errors. In the first step, the equation $S(b) = S_0 \cdot \exp(-bD)$ was fitted to the signals at b = 200 s/mm² and b = 800 s/mm² to obtain the diffusion coefficient D . The intersection of this monoexponential curve with the signal axis was used to obtain $1 - \tilde{f}$, where \tilde{f} is an estimate for the perfusion fraction, which was used to define the bounds. For both the biexponential and triexponential fit, the fit bounds for f , f_1 , and f_2 were set to

0 as the minimum and to 1.5 times the estimated perfusion fraction \tilde{f} as the maximum. The bounds for D^* , D_1^* , and D_2^* were set to (0.01, 20) mm^2/s , (0.005, 0.3) mm^2/s , and (0.15, 20) mm^2/s , respectively. The intervals were chosen quite broadly to minimize the influence on the fit result and to avoid the parameters being equal to a bound. In the second step, these bounds were used to fit S_0 and all IVIM parameters except for D , which was kept constant. As it is not possible to measure with an exact diffusion weighting of zero,³³ it was necessary to also fit the initial signal strength S_0 instead of setting $S_0 = S(b = 0)$. To obtain the most accurate set of fit parameters, the biexponential and triexponential fit were each performed 100 times with different starting points, which were randomly selected in the range between the bounds, and the respective set of fit parameters with the lowest sum-of-squares error was saved. No spatial regularization or regularization along the b-value dimension was used.⁸ For the biexponential fit, data at b-values between 0.3 s/mm^2 and 6 s/mm^2 were not used in order to maintain consistency with previous studies.^{37,38} Each data point was weighted equally, which roughly corresponds to an arithmetic averaging. In an additional evaluation, the signals were averaged geometrically over different diffusion directions (resulting in one signal per b-value) and the same fit was performed.

The reliability of the fit procedure was evaluated with a bootstrap approach.³⁹ For a ROI with n voxels, we sampled the new set of voxels by drawing with replacement n times from the original set of voxels. This means that the new set had also n voxels, with some of the original voxels missing and some of the original voxels being present multiple times. Afterward, the new set of voxels was evaluated analogously to the original one. This resampling (ie, drawing with replacement) was done 1000 times for each ROI, therefore resulting in 1000 sets of IVIM parameters per volunteer and echo time. The ratio of SD, eg, σ_f of the 1000 IVIM parameters and the original parameter value, eg, f , (without resampling) was calculated to assess the reliability.

2.3 | Statistics

Statistical analysis was performed with the Kruskal-Wallis test. This test was used instead of one-way analysis of variance (ANOVA) because a preliminary analysis with the Shapiro-Wilk test showed that a normal distribution could not be assumed for any of the measured parameters. For the post-hoc test, the Dunn-Sidak approach was used to correct the p-value for multiple comparisons. For correlation analysis, we calculated the Pearson correlation coefficient. The significance level for all statistical tests was set to 0.05.

2.4 | T_2 analysis

The two observed pseudodiffusion compartments can possibly be explained by the venous and arterial blood pool. To evaluate this hypothesis, the expected ratio of their signal fractions f_A/f_V was estimated by

$$\frac{f_A}{f_V} = \frac{\exp\left(-\frac{TE}{T_{2,\text{arterial}}}\right)}{\exp\left(-\frac{TE}{T_{2,\text{venous}}}\right)}$$

and was compared to the ratio of f_2 and f_1 . The used values for the relaxation times of arterial and venous blood were $T_{2,\text{arterial}} = 44$ ms and $T_{2,\text{venous}} = 107$ ms.³¹

3 | RESULTS

3.1 | IVIM parameters

Figure 1 shows the results of the phantom measurement at $TE = 45$ ms. The measured diffusion coefficient was $D = (2.0620 \pm 0.0008) \cdot 10^{-3} \text{mm}^2/\text{s}$. The values for D at 60 ms, 75 ms, and 90 ms were $(2.0633 \pm 0.0008) \cdot 10^{-3} \text{mm}^2/\text{s}$, $(2.0655 \pm 0.0008) \cdot 10^{-3} \text{mm}^2/\text{s}$, and $(2.0698 \pm 0.0007) \cdot 10^{-3} \text{mm}^2/\text{s}$, respectively. For all TEs, the measured signals were very close to the expected monoexponential signal decay. The temperature of the phantom was 21.4°C and 22.2°C before and after the measurement, respectively. The expected water diffusion coefficient for these temperatures is between $2.109 \cdot 10^{-3} \text{mm}^2/\text{s}$ and $2.153 \cdot 10^{-3} \text{mm}^2/\text{s}$.⁴⁰

Figure 2 shows representative images acquired at different b-values and TEs. The ROIs for this volunteer were plotted sparing major vessels and the left liver lobe. As the ROI shape was adapted for each TE, a slightly different shape of the ROI at $TE = 45$ ms and $TE = 90$ ms can be perceived.

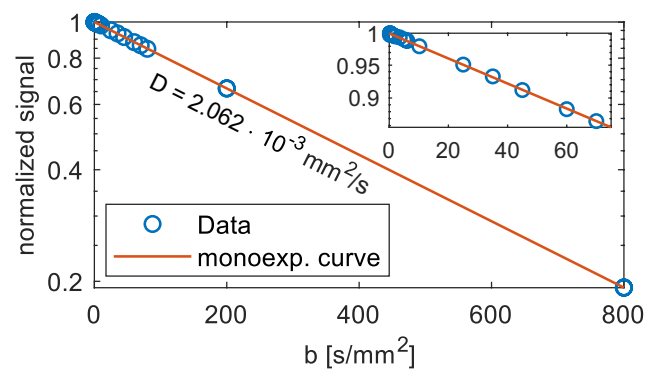


FIGURE 1 Diffusion-weighted signal of a water phantom at $TE = 45$ ms. Data points (blue) and monoexponential fit curve (red) are shown

FIGURE 2 Representative images and ROIs (white outline) at different TEs and b-values. Small TE-dependent changes of the ROI were necessary if additional image artifacts occurred at different TEs or due to subject motion. The signal was plotted in arbitrary units. Note that the images are windowed differently for each TE

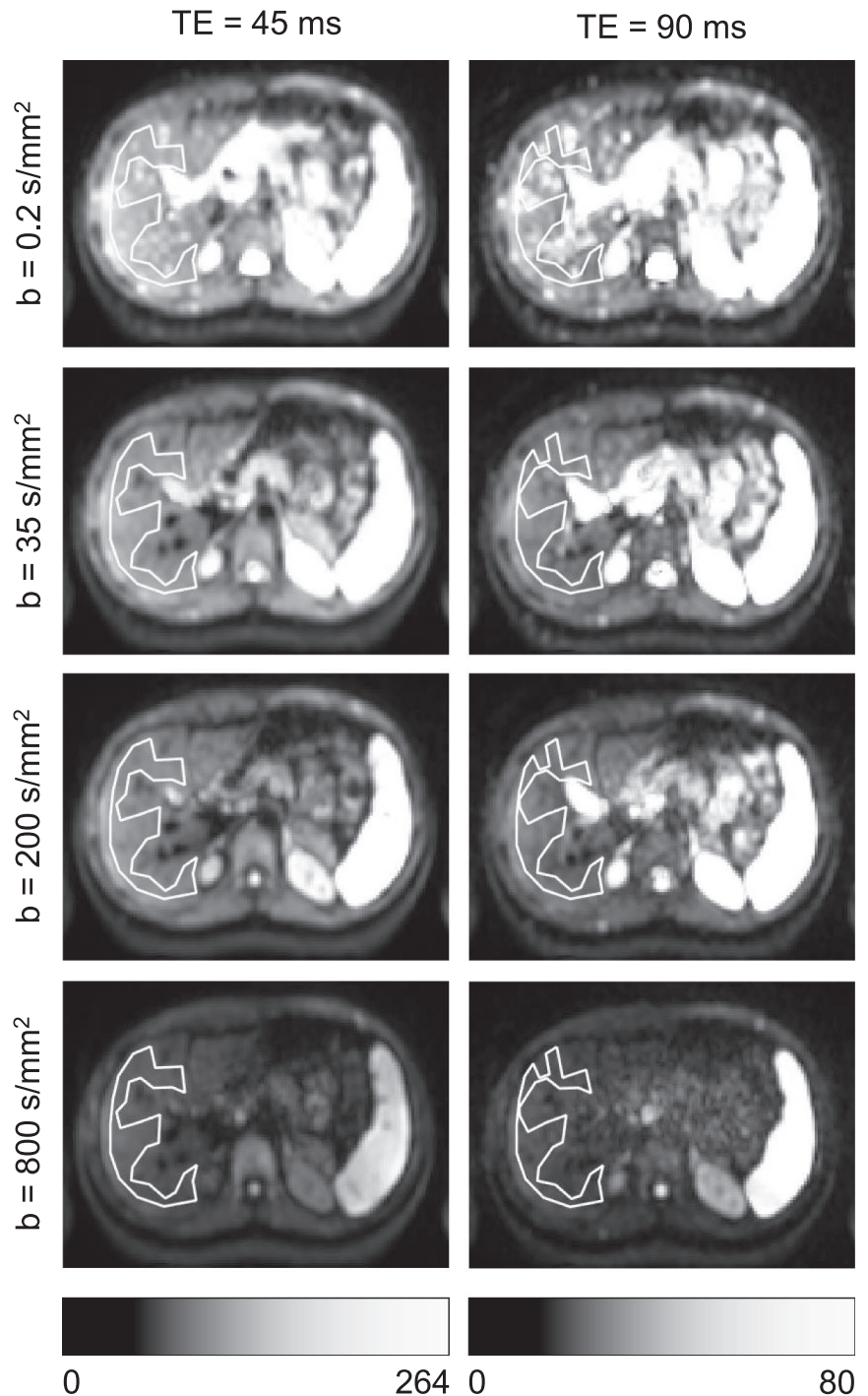


Figure 3 shows the representative measured signals, bi- and triexponential fit curves, and a comparison of the absolute signal curves at the four TEs for one volunteer. The markers that were used only in the triexponential fit are plotted with lower brightness. Both fit curves match the measured data well; only the biexponential fit curve did naturally not match the excluded data points. The signal decreased at longer TE (Figure 3B), but the percentage of the initial signal decay at low b-values became larger, indicating the increased perfusion fractions at longer TE.

The average relative errors, calculated from the errors provided by the fit routine, were: D : 2.6 %, D_1^* : 13.5 %, D_2^* : 21.1 %, f_1 : 6.0 %, f_2 : 9.0 %, D^* : 9.1 %, f : 2.7 %.

The relative error σ_x/x , estimated with the bootstrap approach and averaged over volunteers and TEs, was: D : 0.5 %, D_1^* : 5.6 %, D_2^* : 22.2 %, f_1 : 2.4 %, f_2 : 4.4 %, D^* : 10.3 %, f : 0.9 %. The values for σ_x/x for the parameters D_2^* and D^* each had one single outlier for one volunteer at TE = 60 ms ($\sigma_{D_2^*}/D_2^* = 1050$ %, $\sigma_{D^*}/D^* = 421$ %), leading to the increased averaged ratio. Without these outliers, the averaged ratios were 4.8 % and 3.4 %, respectively.

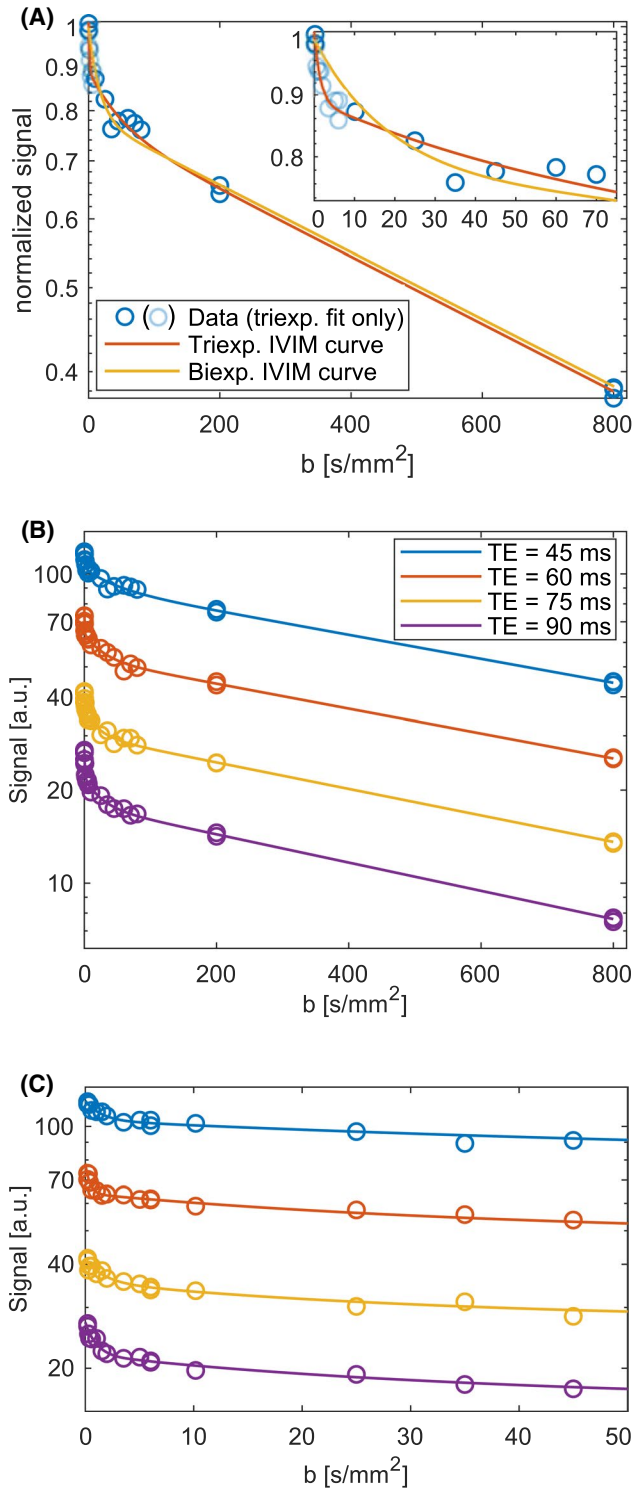


FIGURE 3 Representative diffusion-weighted signal curves measured in the liver of one volunteer. For better readability, the displayed signal values represent the values averaged over diffusion directions and slices. A, Representative normalized signals of one volunteer at TE = 45 ms. Both the biexponential and triexponential fit curves are shown. Data points with lower brightness were used for the triexponential fit only. B, Representative absolute signal of the same volunteer at four TEs. Lines represent the triexponential IVIM curves. C, Enlarged view of subplot B for small b -values

Figure 4 shows the averaged histograms of the parameter distributions. As mentioned above, for both D_2^* and D^* , one of the 60 (15 volunteers, four TEs) calculated relative errors was quite large. The histograms of the distributions leading to these high values are shown as supplemental material (Supporting Information Figure S1, which is available online).

Figure 5 shows the resulting IVIM parameters of the volunteer measurements. For each parameter, box plots at the four TEs are shown. Additionally, Table 1 lists the median values (same underlying data as in Figure 5) and results of the statistical analysis with the Kruskal-Wallis test.

A significant dependency of D , D^* , D_1^* , and D_2^* was not observed. Outliers were more prevalent for the pseudodiffusion coefficients than for the other parameters; in particular for the triexponential pseudodiffusion coefficients. The “slow” triexponential pseudodiffusion coefficient D_1^* was smaller than the biexponential pseudodiffusion coefficient D^* by approximately a factor of two, whereas D_2^* was larger than D^* by approximately a factor of 10.

Both the biexponential and triexponential perfusion fractions were significantly dependent on the TE and increased similarly and approximately by a factor of 2 at the largest TE compared to the smallest TE.

Table 2 shows the results of the post-hoc test, which was performed for parameters that showed TE dependence. For f_1 , a significant change was observed between the TE pairs (45 ms, 90 ms) and (60 ms, 90 ms). For f_2 , the change was significant between the TE pairs (45 ms, 75 ms) and (45 ms, 90 ms). For the biexponential perfusion fraction f , a significant change occurred between the TE pairs (45 ms, 75 ms), (45 ms, 90 ms), and (60 ms, 90 ms).

The Pearson correlation coefficients (IVIM parameter vs. TE) were: f_1 : 0.512 ($P < .001$), f_2 : 0.568 ($P < .001$), f : 0.681 ($P < .001$), D_1^* : -0.085 ($P = .518$), D_2^* : 0.130 ($P = .322$), D^* : 0.136 ($P = .300$), D : -0.083 ($P = 1$).

The results for the geometric averaging were almost identical and are presented in the supplemental material (Supporting Information Figure S2).

3.2 | T_2 analysis

The calculated values for f_A/f_V and the comparison to the ratio of f_2 and f_1 are shown in Table 3. The values for f_A/f_V decrease with increasing TE, the values for f_2/f_1 are nearly constant.

4 | DISCUSSION

In this study, we examined the TE dependence of the biexponential and triexponential IVIM model. The triexponential

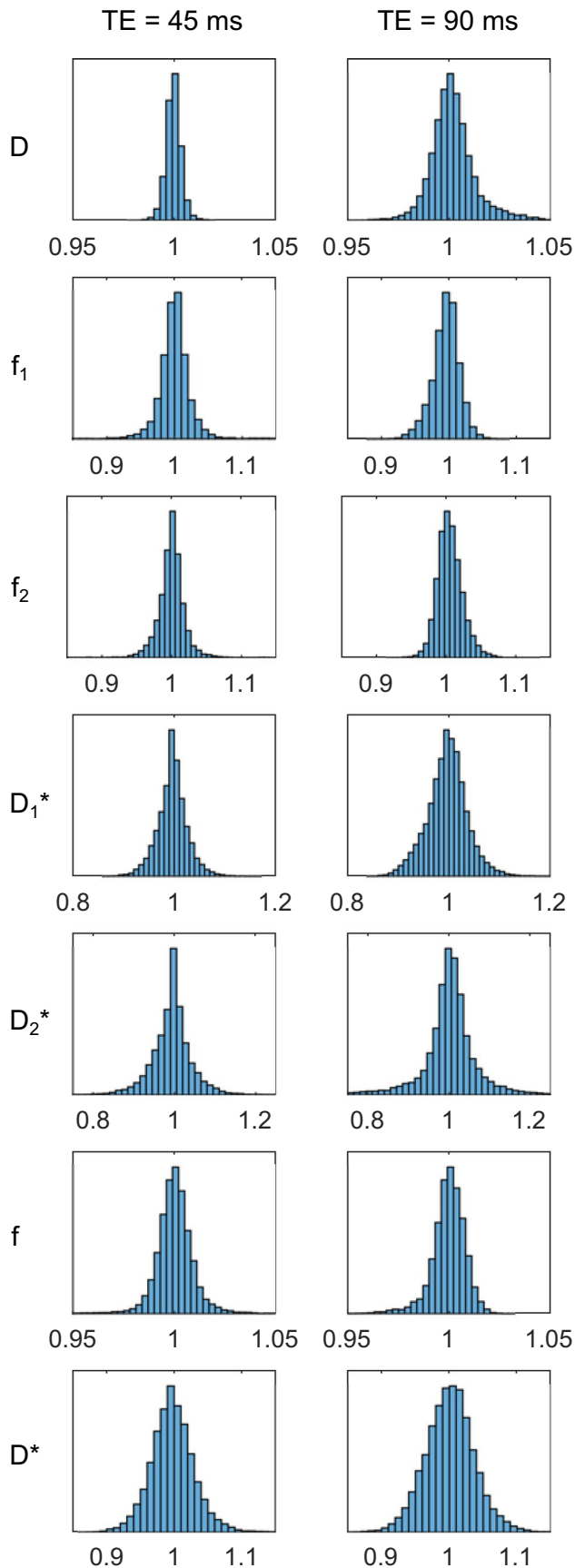


FIGURE 4 Histograms of the parameter distributions obtained with the bootstrap approach. The value on the horizontal axis denotes the ratio between the result of the bootstrap fit and the result of the original fit; that is, a value of 1 means that they are identical. The histograms are shown for TE = 45 ms and TE = 90 ms and are averaged over all volunteers. All histograms are normalized to the value of the respective highest bar

perfusion fractions f_1 and f_2 and the biexponential perfusion fraction f depended significantly on the TE, whereas the diffusion coefficient D , the triexponential pseudodiffusion coefficients D_1^* and D_2^* , and the biexponential pseudodiffusion coefficient D^* did not.

A meta-analysis found that the diffusion coefficient D was $(10.9 \pm 1.7) \cdot 10^{-4} \text{ mm}^2/\text{s}$ if averaged over 27 different healthy liver studies.²⁹ In our study, it lay between $9.4 \cdot 10^{-4} \text{ mm}^2/\text{s}$ and $9.7 \cdot 10^{-4} \text{ mm}^2/\text{s}$, which is within the margin of error of this literature value.

In the same review,²⁹ the perfusion fraction f was given as 0.231 ± 0.085 and the pseudodiffusion coefficient D^* as $(7.0 \pm 3.1) \cdot 10^{-2} \text{ mm}^2/\text{s}$, which is also in line with our results.

Table 4 shows an overview of published triexponential IVIM parameters and of those determined in the present study, a graphical representation is shown in Figure 6. The triexponential perfusion fractions f_1 and f_2 were approximately of equal size in all studies with similar TE. The finding that both values increase with TE is confirmed when the previous reports are considered. One exception to this rule is the study by Riexinger et al⁵ (cf. TE = 100 ms in Figure 6, see below for a further discussion on the values reported in that study).

The value for D_2^* was generally much larger than that for D_1^* . Even the minimal reported ratio D_2^*/D_1^* was > 6 (by Wurnig et al⁷). In all other studies, D_2^* was larger than D_1^* by at least an order of magnitude, which itself was again at least an order of magnitude larger than D . If the average over all reported D , D_1^* , and D_2^* values is taken, then D_1^* is approximately 25 times larger than D ; and D_2^* is approximately 25 times larger than D_1^* .

Our finding that neither D nor the triexponential pseudodiffusion coefficients depended significantly on TE is supported when taking into account previous reports; a dependency on TE is not observable in Table 4. The values for D_1^* and D_2^* seem to be conspicuously high at TE = 60 ms, but the values of the quartiles indicate and the statistical analysis shows that this is no significant effect. Our TE-averaged D_2^* value was larger than those of most other studies, which is presumably caused by the lower b-values used in our study. Interestingly, the D_2^* values reported in a previous study⁵ were even larger. In comparison to our study, one main difference can be identified: In the present study, we used a higher maximal b-value of $800 \text{ s}/\text{mm}^2$ (vs. $500 \text{ s}/\text{mm}^2$). Even though it is often assumed that the kurtosis effect can be neglected for b-values up to $800 \text{ s}/\text{mm}^2$ in abdominal

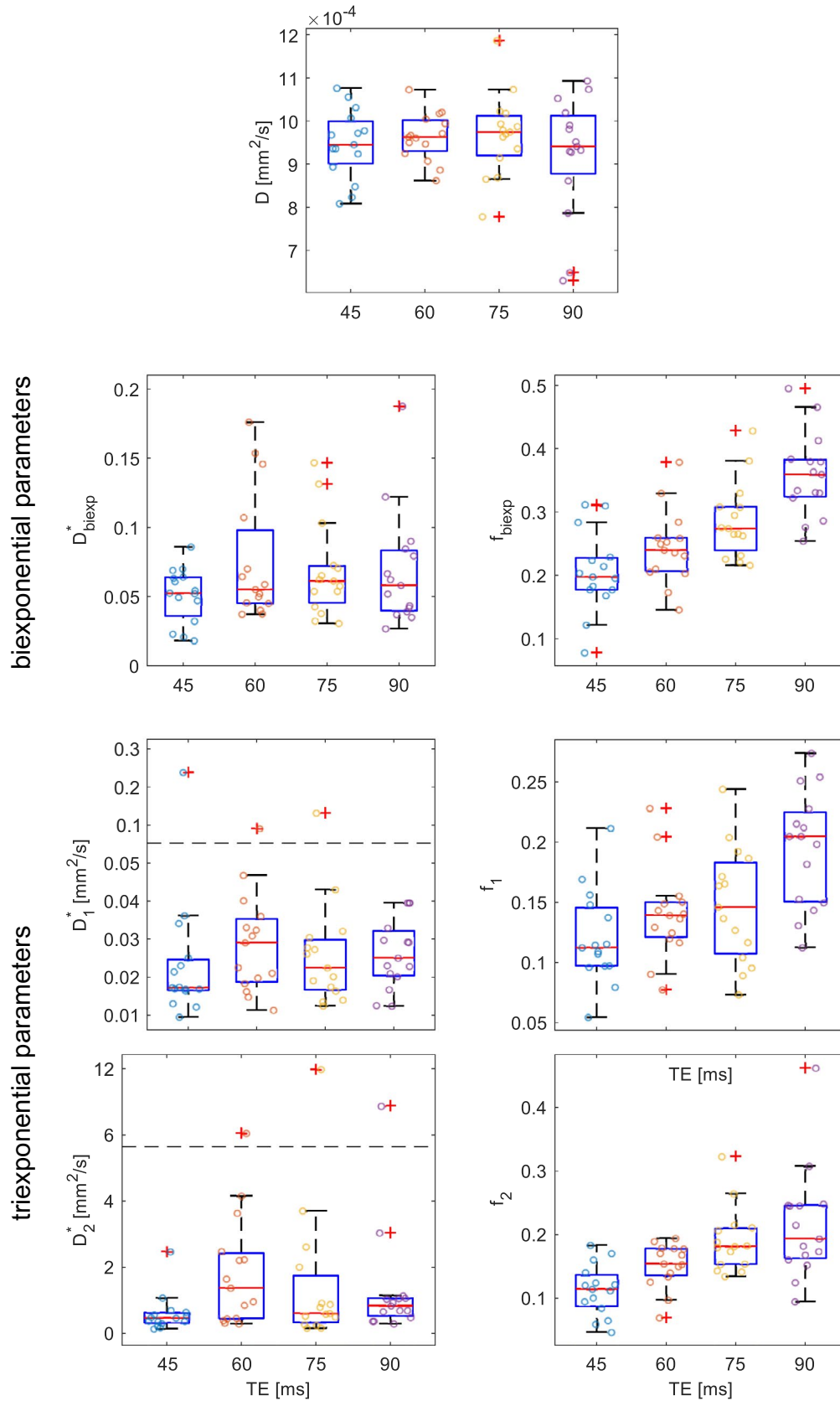


FIGURE 5 Box plots of the bi- and triexponential IVIM parameters. Each point represents the parameter obtained for one volunteer. The central red horizontal line in the box plot indicates the median; the bottom and top lines indicate the 25th and 75th percentile, respectively. The whiskers reach out to $\pm 2.7 \sigma$; “+” indicates outliers. Dashed horizontal lines show the threshold where the scale of the y-axis is changed to display all points in a reasonable manner

TABLE 1 Median of the IVIM parameters at four different TEs (first and third quartiles are stated in brackets) and *P*-values, calculated with the Kruskal-Wallis test

		45 ms	60 ms	75 ms	90 ms	<i>P</i> -Value
<i>D</i>	(10 ⁻⁴ mm ² /s)	9.45 (9.01, 10.0)	9.63 (9.31, 10.0)	9.75 (9.20, 10.1)	9.41 (8.78, 10.1)	.601
<i>D</i> ₁ [*]	(10 ⁻² mm ² /s)	1.73 (1.65, 2.46)	2.91 (1.87, 3.53)	2.25 (1.67, 2.98)	2.51 (2.04, 3.22)	.360
<i>D</i> ₂ [*]	(mm ² /s)	0.478 (0.327, 0.634)	1.38 (0.461, 2.43)	0.616 (0.337, 1.75)	0.846 (0.538, 1.07)	.053
<i>f</i> ₁		0.113 (0.098, 0.146)	0.139 (0.121, 0.150)	0.146 (0.107, 0.183)	0.205 (0.151, 0.225)	.001
<i>f</i> ₂		0.115 (0.086, 0.137)	0.155 (0.136, 0.178)	0.182 (0.154, 0.210)	0.194 (0.163, 0.247)	<.001
<i>D</i> [*]	(10 ⁻² mm ² /s)	5.26 (3.60, 6.40)	5.52 (4.52, 9.80)	6.13 (4.55, 7.21)	5.82 (3.98, 8.33)	.601
<i>f</i>		0.198 (0.177, 0.228)	0.240 (0.207, 0.260)	0.274 (0.239, 0.308)	0.360 (0.324, 0.383)	<.001

TABLE 2 *P*-Values for the perfusion fractions calculated with the post-hoc Dunn-Sidak test

		60 ms	75 ms	90 ms
<i>f</i> ₁	45 ms	0.763	0.549	0.001
	60 ms	—	1.000	0.043
	75 ms	—	—	0.096
<i>f</i> ₂	45 ms	0.200	0.001	< 0.001
	60 ms	—	0.355	0.178
	75 ms	—	—	1.000
<i>f</i>	45 ms	0.735	0.020	< 0.001
	60 ms	—	0.471	0.001
	75 ms	—	—	0.139

TABLE 3 Comparison of calculated *f_A/f_V* and measured *f₂/f₁*

TE (ms)	<i>f_A/f_V</i>	<i>f₂/f₁</i>
45	0.55	1.02
60	0.45	1.12
75	0.37	1.25
90	0.30	0.95

organs,⁷ it might nonetheless have some influence.⁴¹ If this was the case, the signal at high b-values would be larger than expected, leading to a reduced measured diffusion coefficient compared with that at a maximal b-value of 500 s/mm², and may explain the smaller diffusion coefficient in the present study ($D \approx 0.96 \cdot 10^{-3}$ mm²/s) than in the earlier report ($D \approx 1.22 \cdot 10^{-3}$ mm²/s). As a consequence of this smaller *D* value, the extrapolation of the diffusion compartment to the point $b = 0$ will hit the signal axis at a lower point, leading to an increased estimate of the perfusion fractions, which could also have an influence on the pseudodiffusion coefficients. This explanation is supported by the finding that the results of another study by the same researcher¹⁴ and a highest b-value of 800 s/mm² are more in line with our results. Elucidating the dominant mechanism at work here is beyond the scope of the present study and highlights the challenges associated

with obtaining quantitative triexponential IVIM parameters. These challenges are highlighted to an even larger extent if one considers that even the values reported for *D*, which can be estimated most precisely among the IVIM parameters,¹⁴ vary by 30% in the different studies. The exact same handling of all evaluation steps (ROI placement strategy, fitting process, etc.) appears mandatory if true comparability among studies is sought. Moreover, IVIM parameters may differ significantly between MR scanners from different vendors,⁴² which might also be a source of the observed parameter deviations. The evaluation of the fit reliability with the bootstrap approach showed nevertheless that within our study, the averaged relative deviation is smaller than 6% (one outlier left out for *D*^{*} and *D*₂^{*}), indicating that almost all fit results can be considered trustworthy and stable.

The observation that the perfusion fractions *f*₁ and *f*₂ increased with the TE is not unexpected; a similar behavior was observed for the perfusion fraction *f* in the biexponential IVIM model.^{26,27} This can be explained by the different T₂ relaxation times. In the case of the biexponential model, the line of argument is as follows: Blood and liver tissue, which represent the compartments, have different T₂ times, which leads to a TE-dependent value of *f*. With rising TE, the shorter T₂ time of liver tissue makes the signal fraction of the tissue compartment decrease, and an increase of *f* can be observed. For the triexponential model, the parameters *f*₁ and *f*₂ might be represented by different blood compartments and, therefore, may exhibit different T₂ times. Wurnig et al⁷ hypothesized that the compartments might represent arterial and venous blood. Essentially, this would render *f*₁ and *f*₂ dependent on TE in a non-identical manner. At 3T, the T₂ time of venous blood is approximately 44 ms; that of arterial blood is approximately 107 ms.^{5,31} As T_{2,liver} was reported to be 34 ms,⁴³ the perfusion fractions would also increase at larger TEs, but at a very different rate. We observed, however, that the rate of increase was almost equal for *f*₁ and *f*₂, which leads to the conclusion that both compartments have similar T₂ times. The qualitative evaluation strengthens this finding: The ratio of *f*₁ and *f*₂ is nearly constant, whereas the expected ratio decreases by a factor of approximately 2 from lowest to

TABLE 4 Published triexponential IVIM parameters of the liver

Publication units	TE ms	D 10 ⁻³ mm ² /s	D ₁ [*]	D ₂ [*]	f ₁	f ₂	f ₁ +f ₂	b-Values s/mm ²	TR ms	B ₀ T
This study	45	0.95	17.3	478	0.11	0.11	0.22	0.2, ..., 800	1rc	3
Riexinger et al ¹⁴	45	1.10	16	500	0.13	0.11	0.24	0.15, ..., 800	1rc	3
Chevallier et al ⁴	55	0.98	15.1	445	0.12	0.12	0.24	0, 3, 10, 25, ..., 800	2149	3
Wurnig et al ⁷	57	1.26	43.8	270	0.08	0.13	0.21	0, 15, 30, ..., 1005	5300	3
This study	60	0.96	29.1	1385	0.14	0.15	0.29		1rc	3
Cercueil et al ³	67	1.35	26.5	392	0.14	0.14	0.28	0.5,10, ..., 800	1rc	3
Kuai et al ⁵¹	68	1.21	19.3	386	0.17	0.17	0.34	0, 5, 15, ... 800	1rc	3
This study	75	0.97	22.5	616	0.15	0.18	0.33	0.2, ..., 800	1rc	3
This study	90	0.94	25.1	846	0.20	0.19	0.39	0.2, ..., 800	1rc	3
Riexinger et al ⁵	100	1.22	81.3	2453	0.16	0.15	0.31	0.2, ..., 180, 500	2500	3

Abbreviation: 1rc, one respiratory cycle.

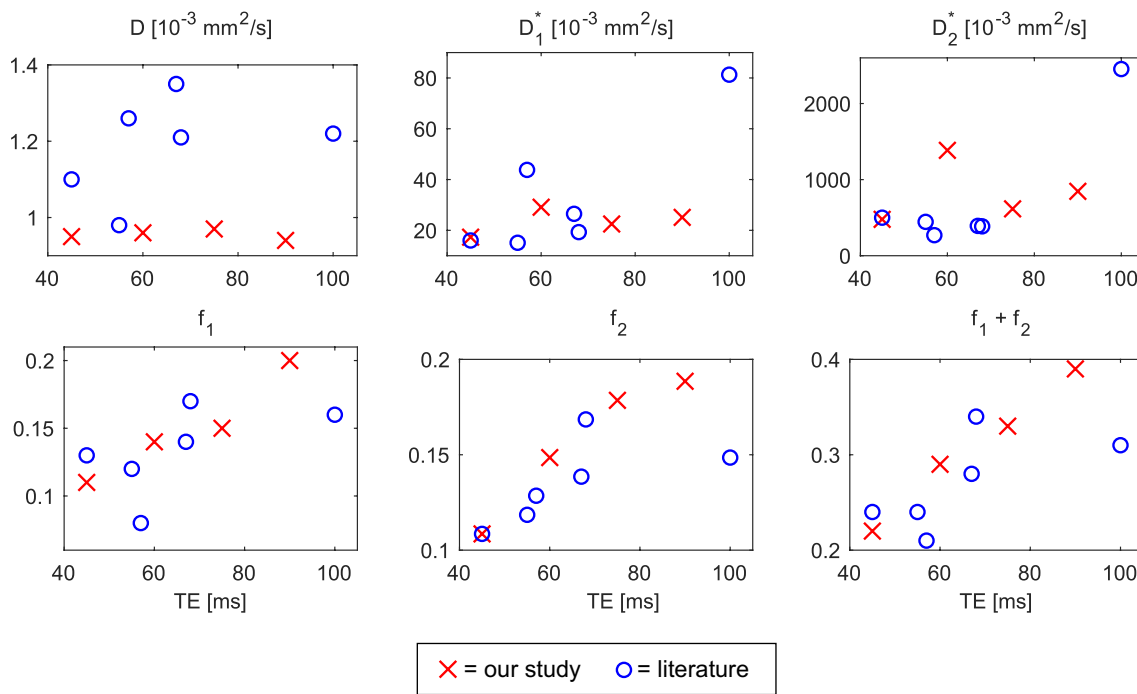


FIGURE 6 Comparison of IVIM parameters at different echo times. Red crosses denote values from our study, blue circles denote values from literature, which are also stated in Table 4

highest TE measured. Note that this evaluation only focusses on the general trend of the expected ratio rather than its exact value. For a more exact quantification, the volume fractions of arterial and venous blood would have to be taken into account. However, these are challenging to determine and may depend on the digestive state.⁴⁴ The general trend allows the presumption that the fast and slow perfusion compartments contain both arterial and venous blood. This agrees with the observation that a field strength dependency of the bi- and triexponential IVIM parameters does not exist,⁵ although

venous and arterial blood exhibited different field strength dependencies in terms of their T₂ times.

It is important to consider the behavior of f₁ and f₂ when the triexponential parameters are used for disease characterization. Absolute values of f₁ and f₂ can only be a reliable source of diagnostic information when the value of TE is taken into account. If different TEs are used, a bias in f ensues if one compares the values directly. This problem could be overcome by defining a standard TE or some form of TE-dependent standard values for f₁ and f₂, but this appears quite

complicated for clinical work. Another approach might be a TE correction strategy as proposed for the biexponential f .²⁶ The development, application, or evaluation of such a correction strategy, however, was beyond the scope of this work.

In contrast, the finding that D^* was not dependent on TE indicates that it is possible to compare this parameter among studies performed with different TEs, which is a notable advantage. The same holds true for the triexponential pseudodiffusion coefficients D_1^* and D_2^* . A correction strategy for these parameters does therefore not seem necessary. However, this must be taken with a grain of salt: The diffusion time in our study was kept constant – an important strategy in order to only detect differences due to changes in TE. For example, this avoided any influence of the diffusion time on the diffusion coefficient D ^{45,46} and on the pseudodiffusion coefficient whose flow correlation time has been reported to be in the order of 100 ms.²⁵ However, many previous studies coupled TE and the duration of the diffusion encoding. A dependence of D_1^* on the time separation Δ of the gradient lobes was, for example, reported by Fournet et al.⁴⁷ Although these measurements were performed in the rat brain, the finding might generalize to further organs and to pathological tissue. For that reason, the use of different TE might still pose some problems concerning the comparability of pseudodiffusion coefficients among studies. Moreover, the large uncertainty associated with the pseudodiffusion parameters should be kept in mind. Potentially, technical improvements will make it possible to measure them with higher precision in the future.

We must also acknowledge several limitations of this study. First, the in-house developed sequence used did not compensate for eddy currents that can induce image distortions.⁴⁸ The volunteers who were scanned stated that they had no history of liver disease. However, the images were only checked for obvious pathologies and not by a radiologist, and pre-existing conditions could have falsified the outcome. Additionally, the volunteers were not obliged to follow a prescribed fasting protocol prior to the measurement; different digestive states might possibly have altered the results. Regarding the ROI placement strategy, the use of smaller ROIs might have reduced the risk to accidentally include vessels, but at the expense of statistical power that was obtained with the larger ROIs used. We tried to minimize a possible influence of undesired very bright or dark voxels by the use of the median for ROI signal evaluation. The use of large ROIs may also lead to averaging regions with different diffusion behavior, in contrast to voxel-wise evaluation, where different regions could possibly have been detected. As there is no general consent about the best fit procedure for IVIM,⁶ a segmented fit was used and considered the most exact, while other fitting algorithms could have yielded different results. Barbieri et al.⁴⁹ reported significant differences in the fit parameters for all upper abdominal organs when they compared

biexponential fitting algorithms. A further possible limitation (see also above) is that we kept the diffusion encoding pulses identical at all TE, while many vendor-provided sequences adapt their duration to that of TE. This may have limited the comparability to other studies, but the advantage is that the TE dependency can be assessed unequivocally. The dependency of IVIM parameters on the timing of the diffusion encoding gradients remains to be investigated in future studies. Our sample size was limited (15 volunteers), and a larger sample size might have revealed statistically significant TE dependencies for the pseudodiffusion compartments. Nonetheless, it was larger than the reported median of six for MRI volunteer studies.⁵⁰


In conclusion, the measured IVIM parameters f , f_1 , and f_2 showed significant dependence on TE, whereas the other IVIM parameters (D , D^* , D_1^* , D_2^*) did not. This indicates that the other IVIM parameters can be compared between studies with different TEs without correction. No indication was found that the two triexponential perfusion compartments represent venous and arterial blood.

ACKNOWLEDGMENTS

Financial support by the Deutsche Forschungsgemeinschaft (LA 2804/12-1, LA 2804/13-1), the Swedish Foundation for Strategic Research (ITM17-0267), and the Swedish Research Council (2018-03697) is gratefully acknowledged.

ORCID

Tobit Führes  <https://orcid.org/0000-0001-6804-6353>

Andreas Julian Riexinger  <https://orcid.org/0000-0002-6346-3526>

[org/0000-0002-6346-3526](https://orcid.org/0000-0002-6346-3526)

REFERENCES

1. Le Bihan D, Breton E, Lallemand D, Grenier P, Cabanis E, Laval-Jeantet M. MR imaging of intravoxel incoherent motions: application to diffusion and perfusion in neurologic disorders. *Radiology*. 1986;161:401-407.
2. Szubert-Franczak AE, Naduk-Ostrowska M, Pasiecz K, Podgorska J, Skrzynski W, Cieszanowski A. Intravoxel incoherent motion magnetic resonance imaging: basic principles and clinical applications. *Pol J Radiol*. 2020;85:e624-e635.
3. Cercueil J-P, Petit J-M, Nougaret S, et al. Intravoxel incoherent motion diffusion-weighted imaging in the liver: comparison of mono-, bi- and tri-exponential modelling at 3.0-T. *Eur Radiol*. 2015;25:1541-1550.
4. Chevallier O, Zhou N, Cercueil JP, He J, Loffroy R, Wang YXJ. Comparison of tri-exponential decay versus bi-exponential decay and full fitting versus segmented fitting for modeling liver intravoxel incoherent motion diffusion MRI. *NMR Biomed*. 2019;32:e4155.
5. Riexinger AJ, Martin J, Rauh S, et al. On the field strength dependence of Bi- and triexponential intravoxel incoherent motion (IVIM) parameters in the liver. *J Magn Reson Imaging*. 2019;50:1883-1892.
6. Chevallier O, Wang YXJ, Guillen K, Pellegrinelli J, Cercueil JP, Loffroy R. Evidence of tri-exponential decay for liver intravoxel

- incoherent motion MRI: a review of published results and limitations. *Diagnostics (Basel)*. 2021;11:379.
7. Wurnig MC, Germann M, Boss A. Is there evidence for more than two diffusion components in abdominal organs? A magnetic resonance imaging study in healthy volunteers. *NMR Biomed*. 2017;31:e3852.
 8. Stabinska J, Ljimini A, Zöllner HJ, et al. Spectral diffusion analysis of kidney intravoxel incoherent motion MRI in healthy volunteers and patients with renal pathologies. *Magn Reson Med*. 2021;85:3085-3095.
 9. van Baalen S, Froeling M, Asselman M, et al. Mono, bi- and tri-exponential diffusion MRI modelling for renal solid masses and comparison with histopathological findings. *Cancer Imaging*. 2018;18:44.
 10. van Baalen S, Leemans A, Dik P, Lilien MR, Ten Haken B, Froeling M. Intravoxel incoherent motion modeling in the kidneys: comparison of mono-, bi-, and triexponential fit. *J Magn Reson Imaging*. 2017;46:228-239.
 11. van der Bel R, Gurney-Champion OJ, Froeling M, Stroes ESG, Nederveen AJ, Krediet CTP. A tri-exponential model for intravoxel incoherent motion analysis of the human kidney: in silico and during pharmacological renal perfusion modulation. *Eur J Radiol*. 2017;91:168-174.
 12. Novikov DS, Kiselev VG, Jespersen SN. On modeling. *Magn Reson Med*. 2018;79:3172-3193.
 13. Lemke A, Stieltjes B, Schad LR, Laun FB. Toward an optimal distribution of b values for intravoxel incoherent motion imaging. *Magn Reson Imaging*. 2011;29:766-776.
 14. Riexinger A, Martin J, Wetscherek A, et al. An optimized b-value distribution for triexponential intravoxel incoherent motion (IVIM) in the liver. *Magn Reson Med*. 2021;85:2095-2108.
 15. Andreou A, Koh DM, Collins DJ, et al. Measurement reproducibility of perfusion fraction and pseudodiffusion coefficient derived by intravoxel incoherent motion diffusion-weighted MR imaging in normal liver and metastases. *Eur Radiol*. 2013;23:428-434.
 16. Zhu LI, Zhu L, Wang H, et al. Predicting and early monitoring treatment efficiency of cervical cancer under concurrent chemoradiotherapy by intravoxel incoherent motion magnetic resonance imaging. *J Comput Assist Tomogr*. 2017;41:422-429.
 17. Yan C, Xu J, Xiong W, et al. Use of intravoxel incoherent motion diffusion-weighted MR imaging for assessment of treatment response to invasive fungal infection in the lung. *Eur Radiol*. 2017;27:212-221.
 18. Chandarana H, Kang SK, Wong S, et al. Diffusion-weighted intravoxel incoherent motion imaging of renal tumors with histopathologic correlation. *Invest Radiol*. 2012;47:688-696.
 19. Klauss M, Mayer P, Maier-Hein K, et al. IVIM-diffusion-MRI for the differentiation of solid benign and malign hypervascular liver lesions-evaluation with two different MR scanners. *Eur J Radiol*. 2016;85:1289-1294.
 20. Pan F, Den J, Zhang C, et al. The therapeutic response of gastrointestinal stromal tumors to imatinib treatment assessed by intravoxel incoherent motion diffusion-weighted magnetic resonance imaging with histopathological correlation. *PLoS One*. 2016;11:e0167720.
 21. Song X-L, Kang HK, Jeong GW, et al. Intravoxel incoherent motion diffusion-weighted imaging for monitoring chemotherapeutic efficacy in gastric cancer. *World J Gastroenterol*. 2016;22:5520-5531.
 22. Wu H, Zhang S, Liang C, et al. Intravoxel incoherent motion MRI for the differentiation of benign, intermediate, and malignant solid soft-tissue tumors. *J Magn Reson Imaging*. 2017;46:1611-1618.
 23. Yiping L, Kawai S, Jianbo W, Li L, Daoying G, Bo Y. Evaluation parameters between intra-voxel incoherent motion and diffusion-weighted imaging in grading and differentiating histological subtypes of meningioma: a prospective pilot study. *J Neurol Sci*. 2017;372:60-69.
 24. Jerome NP, Orton MR, d'Arcy JA, Collins DJ, Koh DM, Leach MO. Comparison of free-breathing with navigator-controlled acquisition regimes in abdominal diffusion-weighted magnetic resonance images: effect on ADC and IVIM statistics. *J Magn Reson Imaging*. 2014;39:235-240.
 25. Wetscherek A, Stieltjes B, Laun FB. Flow-compensated intravoxel incoherent motion diffusion imaging. *Magn Reson Med*. 2015;74:410-419.
 26. Jerome NP, d'Arcy JA, Feiweier T, et al. Extended T2-IVIM model for correction of TE dependence of pseudo-diffusion volume fraction in clinical diffusion-weighted magnetic resonance imaging. *Phys Med Biol*. 2016;61:N667-N680.
 27. Lemke A, Laun FB, Simon D, Stieltjes B, Schad LR. An in vivo verification of the intravoxel incoherent motion effect in diffusion-weighted imaging of the abdomen. *Magn Reson Med*. 2010;64:1580-1585.
 28. Riexinger AJ, Wetscherek A, Martin J, et al. On the magnetic field and echo time dependence of the pseudo-diffusion coefficient. Abstract Number 0258. Presented at: proceedings of ISMRM2018.
 29. Li YT, Cercueil JP, Yuan J, Chen W, Loffroy R, Wang YX. Liver intravoxel incoherent motion (IVIM) magnetic resonance imaging: a comprehensive review of published data on normal values and applications for fibrosis and tumor evaluation. *Quant Imaging Med Surg*. 2017;7:59-78.
 30. Silvennoinen MJ, Clingman CS, Golay X, Kauppinen RA, van Zijl PC. Comparison of the dependence of blood R2 and R2* on oxygen saturation at 1.5 and 4.7 Tesla. *Magn Reson Med*. 2003;49:47-60.
 31. Zhao JM, Clingman CS, Narvainen MJ, Kauppinen RA, van Zijl PC. Oxygenation and hematocrit dependence of transverse relaxation rates of blood at 3T. *Magn Reson Med*. 2007;58:592-597.
 32. Martin J, Endt S, Wetscherek A, et al. Contrast-to-noise ratio analysis of microscopic diffusion anisotropy indices in q-space trajectory imaging. *Z Med Phys*. 2020;30:4-16.
 33. Conturo TE, McKinstry RC, Aronovitz JA, Neil JJ. Diffusion MRI: precision, accuracy and flow effects. *NMR Biomed*. 1995;8:307-332.
 34. Kwee TC, Takahara T, Niwa T, et al. Influence of cardiac motion on diffusion-weighted magnetic resonance imaging of the liver. *MAGMA*. 2009;22:319-325.
 35. Rauh SS, Riexinger AJ, Ohlmeyer S, et al. A mixed waveform protocol for reduction of the cardiac motion artifact in black-blood diffusion-weighted imaging of the liver. *Magn Reson Imaging*. 2020;67:59-68.
 36. Riexinger A, Laun FB, Bickelhaupt S, et al. On the dependence of the cardiac motion artifact on the breathing cycle in liver diffusion-weighted imaging. *PLoS One*. 2020;15:e0239743.
 37. Wurnig MC, Kenkel D, Filli L, Boss A. A standardized parameter-free algorithm for combined intravoxel incoherent motion and diffusion kurtosis analysis of diffusion imaging data. *Invest Radiol*. 2016;51:203-210.
 38. Luciani A, Vignaud A, Cavet M, et al. Liver cirrhosis: intravoxel incoherent motion MR imaging—pilot study. *Radiology*. 2008;249:891-899.
 39. Efron B. Bootstrap methods: another look at the jackknife. *Ann Stat*. 1979;7:1-26.
 40. Mills R. Self-diffusion in normal and heavy water in the range 1–45. deg. *J Phys Chem*. 1973;77:685-688.

41. Filli L, Wurnig M, Nanz D, Luechinger R, Kenkel D, Boss A. Whole-body diffusion kurtosis imaging: initial experience on non-Gaussian diffusion in various organs. *Invest Radiol.* 2014;49:773-778.
42. Barbieri S, Donati OF, Froehlich JM, Thoeny HC. Comparison of intravoxel incoherent motion parameters across MR imagers and field strengths: evaluation in upper abdominal organs. *Radiology.* 2016;279:784-794.
43. de Bazelaire CM, Duhamel GD, Rofsky NM, Alsop DC. MR imaging relaxation times of abdominal and pelvic tissues measured in vivo at 3.0 T: preliminary results. *Radiology.* 2004;230:652-659.
44. Schalkx HJ, Petersen ET, Peters NHGM, et al. Arterial and portal venous liver perfusion using selective spin labelling MRI. *Eur Radiol.* 2015;25:1529-1540.
45. Sen PN. Time-dependent diffusion coefficient as a probe of geometry. *Concepts Magn Reson Part A.* 2004;23A:1-21.
46. Laun FB, Kuder TA, Zong F, Hertel S, Galvosas P. Symmetry of the gradient profile as second experimental dimension in the short-time expansion of the apparent diffusion coefficient as measured with NMR diffusometry. *J Magn Reson.* 2015;259:10-19.
47. Fournet G, Li JR, Cerjanic AM, Sutton BP, Ciobanu L, Le Bihan D. A two-pool model to describe the IVIM cerebral perfusion. *J Cereb Blood Flow Metab.* 2017;37:2987-3000.
48. Finsterbusch J. Eddy-current compensated diffusion weighting with a single refocusing RF pulse. *Magn Reson Med.* 2009;61:748-754.
49. Barbieri S, Donati OF, Froehlich JM, Thoeny HC. Impact of the calculation algorithm on biexponential fitting of diffusion-weighted MRI in upper abdominal organs. *Magn Reson Med.* 2016;75:2175-2184.
50. Hanspach J, Nagel AM, Hensel B, Uder M, Koros L, Laun FB. Sample size estimation: current practice and considerations for original investigations in MRI technical development studies. *Magn Reson Med.* 2020;85:2109-2116.
51. Kuai ZX, Liu WY, Zhu YM. Effect of multiple perfusion components on pseudo-diffusion coefficient in intravoxel incoherent motion imaging. *Phys Med Biol.* 2017;62:8197-8209.

SUPPORTING INFORMATION

Additional Supporting Information may be found online in the Supporting Information section.

FIGURE S1 Bootstrap approach: Histograms of the single volunteer outlier distributions for D_2^* and D^* . The value on the horizontal axis denotes the ratio between the result of the bootstrap fit and the result of the original fit; ie, a value of 1 means that they are identical. The histograms are normalized to the value of the respective highest bar

FIGURE S2 Results with (left) and without (right) geometric averaging of the different diffusion encoding directions

How to cite this article: Führes T, Riexinger AJ, Loh M, et al. Echo time dependence of biexponential and triexponential intravoxel incoherent motion parameters in the liver. *Magn Reson Med.* 2021;00:1–13. <https://doi.org/10.1002/mrm.28996>